

# Multipath Mitigation Technology-integrated GNSS Direct Position Estimation Plug-in Module

Sergio Vicenzo<sup>1</sup> (ORCID: 0000-0003-2974-7899), Bing Xu<sup>1</sup>

<sup>1</sup>Department of Aeronautical and Aviation Engineering, The Hong Kong Polytechnic University, Hong Kong SAR, China

\*Correspondence: Bing Xu (E-mail: pbing.xu@polyu.edu.hk), The Hong Kong Polytechnic University, Hong Kong SAR, China

## Abstract

Direct position estimation (DPE) is an effective solution to the MP issue at the signal processing level. Unlike two-step positioning (2SP) receivers, DPE directly solves for the receiver position, velocity, and time (PVT) in the navigation domain, without the estimation of intermediate measurements, thus allowing it to provide more robust and accurate PVT estimates in the presence of multipath (MP) and weak signals. But GNSS positioning with DPE is mostly left unapplied commercially, and continuing research into DPE has remained relatively stagnant over the past few years. To encourage further research on DPE by the GNSS community, we propose a DPE plug-in module that can be integrated into the conventional 2SP software-defined receivers (SDRs). Programmed in MATLAB, the proposed DPE plug-in module is aimed for better understanding and familiarity of a practical implementation of DPE. Its plug-in module architecture allows it to be incorporated with 2SP MATLAB SDRs, both vector tracking and scalar tracking with minimum changes, making it easy to use, and provides greater flexibility for researchers using various 2SP SDRs. Since the proposed DPE implementation makes use of tracking observables from 2SP to propagate the channel, we propose to further improve the performance of DPE against MP through using MP-compensated observables generated from Multipath Mitigation Technology (MMT)-aided tracking. Referred to as Multipath Mitigation Technology (MMT)-integrated DPE, it is proposed as a variant of DPE that is better suit for urban environment applications. Results show that while in MP-only conditions, an MMT-integrated 2SP has similar performance with MMT-integrated DPE, the proposed MMT-integrated DPE manages to show great superiority against non-line-of-sight (NLOS), making it the preferable option for applications in urban environments.

## Keywords

Global navigation satellite system, Direct position estimation, Non-line-of-sight, Multipath, Urban positioning and navigation, Multipath mitigation technology

## Introduction

The Global Navigation Satellite System (GNSS) is among the most highly relied on navigation and positioning systems in the world. From opening Google Maps to explore new cities during vacations to driving autonomous cars, most layman people do not realize how much they rely on GNSS in their everyday lives. That being said, GNSS often falters in densely populated areas, such as Hong Kong and Tokyo. High-rise buildings and other urban structures typically reflect GNSS signals before reaching the

receiver, generating errors in the pseudorange measurements that may induce errors up to 50 meters (Hsu 2018). When only the reflected signal is received, it is classified as a non-line-of-sight (NLOS) reception. If a combination of the line-of-sight (LOS) and NLOS is received, it is categorized as a multipath (MP) reception. NLOS occurs when the receiver does not have a LOS view to the satellite, while MP signals are usually received when the receiver has LOS view to the satellite but is located close to urban structures e.g., buildings.

Various research has delved into solving the issue of MP and NLOS in GNSS positioning. Several researchers have proposed using 3D mapping-aided (3DMA) GNSS to identify and correct MP and NLOS errors. For example, Ng et al. (2020) proposed the use of 3DMA to generate a skymask (a skymask-based 3DMA) and detect the reflection points for NLOS signals to correct the induced NLOS errors. Results pointed out that a skymask-based 3DMA manages to maintain a positioning accuracy within 10 metres of error in dense urban areas (Ng et al. 2020). A more recent study was to use single-differenced residuals to generate a range residual map to solve for MP/NLOS by analysing the graphical characteristics of MP/NLOS errors (Xu et al. 2024).

The use machine learning methods to detect and mitigate MP errors have also been previously investigated. Phan et al. (2012) employed a support vector regression (SVR) to estimate multipath error by making use of the function between multipath error and satellite relative elevation angle and azimuth angle. On the other hand, Orabi et al. (2020) proposed a neural network-based delay-locked loop (NNDLL), which builds a neural network discriminator using multilayer perceptron (MLP) to estimate code phase directly. Li et al. (2022) also proposed a Deep Neural Network (DNN)-based correlators to mitigate MP effects at two-step positioning (2SP) tracking level through “cleaning” the Autocorrelation function (ACF) from distortions caused by MP.

Closas et al. (2007), on the other hand, proposed to solve the problem at the signal processing level by introducing direct position estimation (DPE). Differing from the conventional 2SP which first estimates the intermediate parameters i.e., pseudoranges and pseudorange rate to produce a position, velocity, and timing (PVT) estimates, DPE estimates the PVT “direct”-ly in the navigation domain using the maximum likelihood principle. By non-coherently combining the satellites correlations, DPE has been shown to offer more accurate PVT estimates against 2SP in cases of weak signals and MP (Axelrad et al. 2009, 2011; Closas and Gusi-Amigó 2017; Closas et al. 2009, 2015). However, GNSS positioning with DPE is mostly left uninvestigated and unapplied commercially, with only one notable commercial receiver that uses DPE (Dampf et al. 2018). One of the possible reasons is its difficult practical implementation. To encourage further research on DPE by the GNSS community, an open-source DPE implementation is proposed. To the best of the author’s knowledge, there has been only one other open-sourced DPE receiver, that is from Peretic and Gao (2021), which was programmed in Python and C++.

Instead of proposing a standalone software-defined receiver (SDR), DPE was proposed as a plug-in module that can be easily integrated into open-sourced 2SP MATLAB SDRs. Tracking data from 2SP is used to propagate the channel for DPE. The aim of the proposed DPE plug-in module is for the familiarization and popularization of DPE in the GNSS community. Proposing DPE as a “plug-in module” permits ease of use for those unfamiliar with DPE, and greater flexibility, since it can be integrated into any MATLAB 2SP SDR, instead of being a separate SDR like Peretic

and Gao's (2021) DPE. Even though the proposed plug-in module is programmed using MATLAB, users can easily translate the code to be integrated into other 2SP SDRs in other programming languages. The DPE plug-in module is currently integrated with the GPS L1 C/A SoftGNSS MATLAB 2SP Scalar Tracking Loop (STL) SDR by Borre et al. (2007), and has been made available at GitHub (<https://github.com/Sergio-Vicenzo/GPSL1-DPEmodule>). Even though the proposed DPE is currently integrated into an STL SDR, integration of the DPE module is not restricted to an STL-based 2SP SDR and it is completely possible to integrate the DPE module into SDRs with other 2SP algorithms such as vector tracking loop (VTL). In addition, it is extendable to other constellations such as BeiDou.

Though DPE has been proven to be robust against MP, previous research has proved that its superior performance against 2SP typically falters in deep urban environments where MP and NLOS are the majority of signals received (Vicenzo et al. 2023). This does not necessarily mean that the performance of DPE is worse than 2SP, but rather that its performance is depreciated to a large degree with increasing errors from MP and NLOS the same way 2SP does. Tang et al. (2024) had also recently showed that while DPE remains more accurate in comparison to 2SP in harsh cases such as 4 out of 8 satellites being MP, DPE error still reaches up to tens, or even hundreds of meters with NLOS measurements, which makes it definitely unsuitable for urban positioning. With research into mitigating MP with 2SP has been widely explored, the prevalence and need for DPE as a robust positioning method against MP has diminished significantly, especially with its high computational load and inapplicability to commercial receivers producing RINEX-level measurements.

To solve this issue for DPE, the second contribution is to introduce a Multipath Mitigation Technology (MMT)-integrated DPE. MMT was introduced as an efficient estimator for accurate estimation of the code delays and carrier phase of the LOS and reflected signal (Weill 2002). In 2SP, the natural way to apply MMT is to integrate it at the tracking stage, replacing the discriminator. Since the proposed DPE implementation made use of 2SP tracking to propagate the channel, we extended the proposed DPE to use the code delays estimated from an MMT-aided tracking to act as the reference code delay for the peak of the ACF. Since DPE traditionally does not require estimation of code delays, the MMT-integrated DPE is proposed as a variant of DPE instead, one that is specifically designed for urban environments. The performance of the proposed MMT-integrated DPE is evaluated with real GNSS urban data, as well as simulated urban datasets produced by a high-end GNSS simulator. Its performance is also compared to an MMT-integrated scalar tracking Least Squares (LS) positioning solution to represent an MMT-integrated 2SP. Similarly with the conventional DPE plug-in module, the MMT-integrated DPE has been made available at GitHub (<https://github.com/Sergio-Vicenzo/GPSL1-MMT-DPEmodule>).

In the following, the basic principles of DPE are introduced first, followed by the architecture of the proposed DPE plug-in module. Next, the principle of MMT is introduced, and the proposed MMT-integrated DPE is presented. The methodology of data collection and results of the proposed DPE and MMT-integrated DPE with both real and simulated GNSS data are then presented and discussed, continued with the conclusion of the findings.

## Modelling of Direct Position Estimation

The idea of DPE solving the PVT directly in the navigation domain is based on the fact that the code phase and Doppler frequency of a GNSS signal can be made as functions of the user PVT. Typically in 2SP, pseudoranges and pseudorange rates are estimated based on tracking measurements of the received signal and from there, the PVT is produced. The concept of DPE reverses this notion. Instead of estimating the received signal parameters i.e., code phase and Doppler frequency (through tracking in 2SP), the PVT acts directly as the variable to be estimated. As a specific PVT corresponds to a specific code phase and Doppler frequency, its corresponding signal replica can be generated and correlated with the incoming signal. Its correlation value determines how likely a candidate PVT is being the receiver PVT. Thus, in a way, rather than estimating the received signal parameters, DPE directly finds the PVT with the code phase and Doppler frequency that “matches” the best with that of the received signal. Recently, Tang et al. (2023) have noted that DPE can also be implemented with carrier phase measurements for greater positioning accuracy. But only the code phase and Doppler frequency measurements are considered for DPE here i.e., the original DPE implementation. This requires the generation of potential PVTs (candidate PVTs), which in this research, is initialized with 2SP PVT estimates (Closas and Gao 2020).

For this research, DPE uses the grid-based method, by which of establishing a set of candidate PVTs and obtaining the correlations from each satellite before finally non-coherently summing them up to obtain the candidate position with the highest signal correlation, which is considered the PVT estimate of DPE. The process is illustrated by the following cost function (Closas and Gao 2020).

$$\hat{\boldsymbol{\gamma}} = \arg \max_{\boldsymbol{\gamma}} \sum_{i=1}^M \|\mathbf{x}^H \mathbf{c}_i(\boldsymbol{\gamma})\|^2 \quad (1)$$

where  $\hat{\boldsymbol{\gamma}} = [p_x, p_y, p_z, \delta t]^T$  are DPE estimates, in which  $\mathbf{p} = [p_x, p_y, p_z]$  is the receiver position in Earth-Centered-Earth-Fixed (ECEF) coordinates and  $\delta t$  is the receiver clock bias.  $\mathbf{x}^H$  is the Hermitian transpose of the received signal vector, denoted by  $\mathbf{x} =$

$\begin{bmatrix} \mathbf{x}[0] \\ \vdots \\ \mathbf{x}[\Delta T - \frac{1}{f_s}] \end{bmatrix}$  and for an L1 C/A signal, each element of  $\mathbf{x}$  is samples of the received baseband signal, presented as the following (Peretic 2019).

$$x(n) = \sum_{i=1}^M a^i s^i \{ (f_{C/A} + f_{\text{code},t}^i) n + \phi_{\text{code},t}^i \} \exp\{ j2\pi (f_{L1} + f_{\text{carr},t}^i) n + \phi_{\text{carr},t}^i \} + \text{noise} \quad (2)$$

in which each element of  $\mathbf{x}$  is referenced to time  $t$  at the start of the sampling window.  $M$  is the total number of satellites in view,  $a^i$  and  $s^i$  are the  $i$ -th satellite amplitude and navigation data spread by the ranging code, respectively (Closas and Gusi-Amigó 2017; Peretic and Gao 2021).  $f_{C/A}$  is the chipping rate of the spreading code of an L1 C/A signal.  $n$  is the index for every element of  $\mathbf{x}$ , with  $n = [0, \frac{1}{f_s}, \frac{2}{f_s}, \dots, \Delta T - \frac{1}{f_s}]$ ,  $f_s$  is the sampling frequency and  $\Delta T$  is the sampling window or coherent integration time (Peretic 2019).  $\phi_{\text{code},t}^i$  and  $\phi_{\text{carr},t}^i$  are the code phase in units of chips and carrier phase in radians of satellite  $i$  at the current measurement sample time,  $t$ , respectively.  $f_{L1}$  is the L1 channel carrier frequency i.e., 1575.42 MHz, and  $f_{\text{code},t}^i$  and  $f_{\text{carr},t}^i$  are the code and carrier frequencies of satellite  $i$  at time  $t$ , respectively. *noise* represents the thermal noise of  $x(n)$  and is assumed to follow the Additive White Gaussian Noise (AWGN).

On the other hand,  $\mathbf{c}_i(\mathbf{y}_j)$  is the vector of locally generated signal replica for satellite  $i$

$$\text{at the } j\text{-th candidate position, denoted by } \mathbf{c}_i(\mathbf{y}_j) = \begin{bmatrix} \mathbf{c}_i[\mathbf{y}_j, 0] \\ \vdots \\ \mathbf{c}_i[\mathbf{y}_j, \Delta T - \frac{1}{f_s}] \end{bmatrix}.$$

### Proposed DPE plug-in module

This section will elaborate how the DPE plug-in module is integrated with the open-source GPS L1 C/A 2SP STL MATLAB SDR (SoftGNSS) (Borre et al. 2007). 2SP information, namely tracking code phase i.e.,  $\phi_{\text{code},t}^i$ , signal transmission time, receiver local time i.e.,  $t$ , satellite position from Least Squares, satellite clock bias, and Least Squares position solution, are used as input for the plug-in module. It might sound counterintuitive to use 2SP tracking estimates for DPE as DPE is supposed to be a single-step positioning algorithm that does not involve tracking. But the use of tracking measurements is merely for channel propagation (and ephemeris decoding in the 2SP part) in the intermediate frequency (IF) data. The possibility of using a tracking loop for propagating the IF channel has also been previously highlighted by Peretic (2019), who had developed his own open-source DPE SDR. A similar approach had also been previously introduced by Closas et al. (2015), who proposed using the delay locked loop (DLL) and phase lock loop (PLL) from 2SP tracking to synchronize the time and code phase. A flowchart detailing how the plug-in module is integrated into the SoftGNSS SDR is shown in Fig. 1.

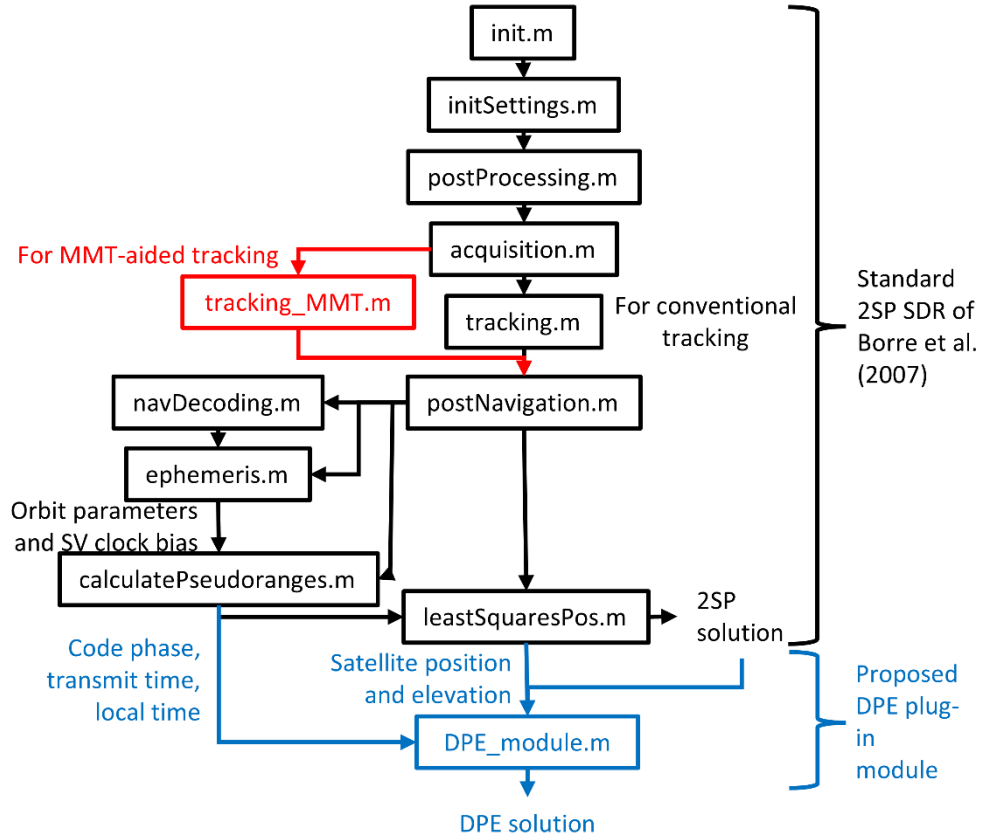


Fig. 1 Flow chart of the proposed DPE plug-in module.

The proposed DPE module utilizes tracking measurements to generate the locally generated signal replicas for each candidate PVT,  $\mathbf{c}_i(\mathbf{y}_j)$ . More specifically, each element of  $\mathbf{c}_i$  will be presented as

$$\mathbf{c}_i(\mathbf{y}_j, n) = s^i \left\{ (f_{C/A} + f_{\text{code},t}^i)n + \phi_{\text{code},t}^i + \Delta\phi_{\mathbf{y}_j}^i \right\} \exp\{j2\pi(f_{L1} + f_{\text{carr},t}^i)n + \phi_{\text{carr},t}^i\} \quad (3)$$

where  $\Delta\phi_{\mathbf{y}_j}^i$  is the difference in code phase between a specific candidate position with the estimated code phase at time  $t$ , which is computed with the following equation (Peretic and Gao 2021):

$$\Delta\phi_{\mathbf{y}_j}^i = -f_{C/A}(t - t_{\text{transmit}}^i) + \frac{f_{C/A}}{c} (\|\mathbf{p}^i - \mathbf{p}_j\| + (\delta t_j - \delta t^i) \cdot c + I + T) \quad (4)$$

where  $t_{\text{transmit}}^i$  is the transmission time of satellite  $i$ .  $\mathbf{p}^i$  and  $\mathbf{p}_j$  are the  $i$ -th satellite and  $j$ -th candidate position ECEF coordinates, respectively.  $\delta t^i$  and  $\delta t_j$  are the  $i$ -th satellite clock bias as well as the  $j$ -th candidate position clock bias, respectively.  $I$  and  $T$  are the ionospheric and tropospheric errors in units of meters, respectively, and  $c$  is the speed of light (Peretic 2019). As seen in (1)-(4), the proposed DPE is currently configured to only estimate the receiver position and clock bias. As noted by Peretic and Gao (2021), estimation of position and velocity parameters can be decoupled. Thus, estimation of velocity parameters is not considered in this paper.

For (3),  $\phi_{\text{code},t}^i$  is obtained from *calculatePseudoranges.m*, which is the function for calculating pseudoranges, while  $f_{\text{code},t}^i$ ,  $f_{\text{carr},t}^i$  and  $\phi_{\text{carr},t}^i$  are directly taken from the tracking function, *tracking.m*. Parameters for (4) i.e.,  $t_{\text{transmit}}^i$ ,  $\mathbf{p}^i$ ,  $\delta t^i$ , and  $T$  are obtained from two-step positioning navigation estimates. Satellite elevation, to be used to correct the tropospheric error, as well as  $\mathbf{p}^i$ , compensated for the Earth rotation are obtained from the function, *leastSquares.m*.  $t_{\text{transmit}}^i$  and  $t$ , which are used to generate pseudoranges in 2SP, are obtained from *calculatePseudoranges.m*.  $t$ , which represents the local time in SoftGNSS, is kept uncompensated from Least Squares clock bias. Position as well as receiver clock bias estimate from *leastSquares.m* are also used as initialization for the grid of candidate position. Since the SoftGNSS codes were not configured to output the aforementioned parameters originally, the codes need to be slightly modified to output the required parameters for the DPE plug-in module.

The grid of candidate PVTs are by default configured to have 1 meter spacing between them. The grid spacing for the latitude-longitude-height estimation can be changed from *initSettings.m* under the parameter *settings.candPVT\_spacing*. Yet, the spacing between the clock bias candidates is fixed at 1 meter. The PVT search space is set to have a span of  $\pm 30$  meters for the latitude and longitude search space,  $\pm 50$  meters for the height search space, and  $\pm 20$  meters for clock bias by default. The candidate PVTs are centered around 2SP PVT estimate for every epoch to avoid DPE estimates from diverging in cases of strong interference or MP or NLOS effect.

The search space span can be edited in *initSettings.m* under the parameters *settings.DPE\_latlong\_span*, *settings.DPE\_height\_span*, and *settings.DPE\_clkBias\_span* (the parameter names are self-explanatory). The non-coherent integration time for DPE can also be changed through *initSettings.m* under the parameter *settings.DPE\_nonCohInt* to improve the performance of DPE as the satellite

correlations will be more filtered. But since DPE is to be compared with 2SP, both coherent and non-coherent integration time is 1 ms for both DPE and 2SP to allow an apple-to-apple comparison. The DPE-integrated SoftGNSS SDR requires ground truth coordinates in geodetic coordinates to output the positioning errors from both DPE and 2SP. Ground truth coordinates are labelled as *settings.gt\_llh* at *initSettings.m*.

The proposed DPE can also be set to output the correlograms, plotted at the estimated DPE height, for each of the satellite correlations as well as the resulting non-coherent sum over the navigation domain (parameter *settings.DPE\_plotCorrelogram*). Samples of the correlograms are shown in Fig. 2 below.

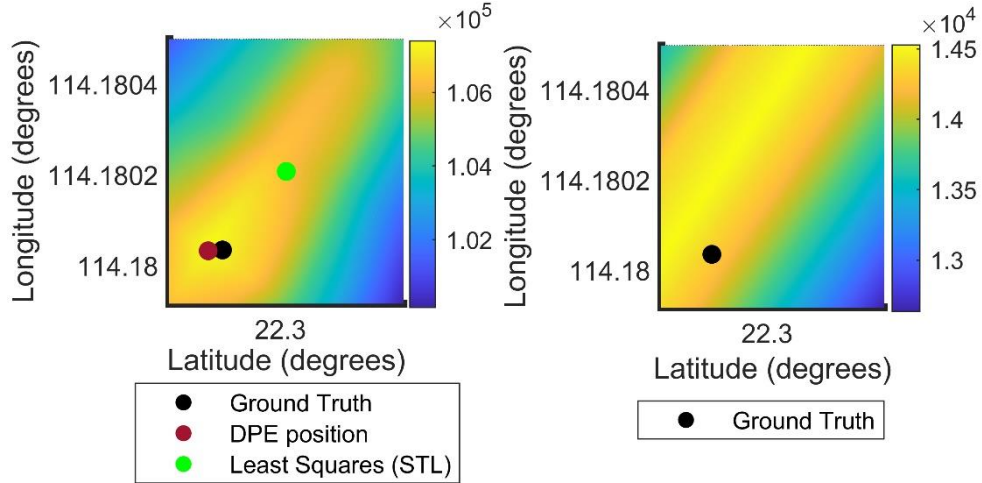


**Fig. 2** The final correlogram after summing up individual satellite correlations (Left) and the correlogram of a single satellite (Right), plotted across degrees latitude and longitude at estimated DPE height.

Instead of iteratively computing the signal correlations per every candidate position, the DPE plug-in module pre-calculates the correlations per every pre-determined chip spacing or code phase. This implementation was previously used by previous research on collective detection, which is another name for DPE, to save computational time (Axelrad et al. 2009, 2011; Cheong et al. 2011; Li et al. 2013). Since the pre-calculated correlations correspond to a specific code phase, the correlations for every candidate position are later given based on its code phase. Since it is virtually impossible to pre-calculate the correlations that fit perfectly to every candidate position code phase, the correlations will be interpolated. A loss in accuracy is expected from the use of interpolation. But due to the limitation from the front-end sampling frequency, code phases within the same samples spacing bear the same correlation value. For example, a front-end with sampling frequency  $f_s = 20$  MHz bears approximately  $20 \text{ MHz} / 1.023 \text{ MHz} = 19.55$  samples/chip or 0.05115 chips/sample for an L1 C/A signal. So, code phases within 0.05115 bears the same correlation value. If correlations are done at spacings narrower than the chips/sample value, the resulting ACF is “zig-zaggy”. Thus, to prevent loss in accuracy, and at the same time preventing a “zig-zaggy” pre-calculated correlations, the pre-calculated correlations are done at spacings of chips/sample, computed with  $f_{C/A}/f_s$  by default. For flexibility, the spacings between the pre-calculated correlations can be changed through *initSettings.m* under the parameter *settings.chipspacing\_dpe\_precalc*. In a way, the use of interpolation with the pre-calculated correlations can be seen as filtering the correlogram over candidate positions, since iteratively computing the signal correlations per every candidate position empirically bear a “zig-zaggy” correlogram.

## Multipath Mitigation with DPE

Before exploring into the proposed MMT-integrated DPE, the basics of how the proposed DPE plug-in module architecture can outperform 2SP against MP will first be explained. As mentioned above, the implementation of DPE will first pre-calculate the correlations per every code phase, with the code phase referenced to that produced from tracking. An illustration of the process is provided in the figure below.

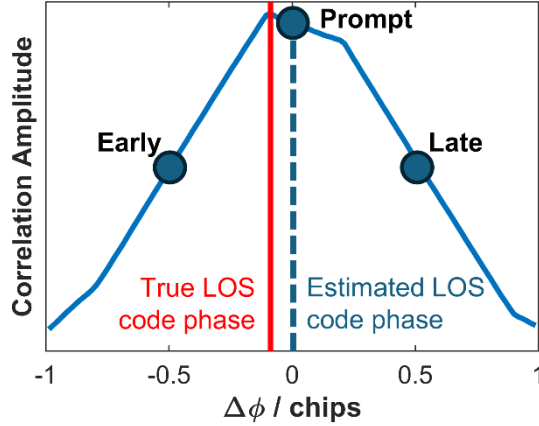


**Fig. 3** Relationship between  $\Delta\phi$  and correlation value of a constructive MP-affected ACF in 2SP tracking. In this case, the relative amplitude of the reflected signal is less than the LOS path.

It is well known that MP deforms the ACF, which introduces errors in tracking (Xu et al. 2019b). Since the tracking loops aim to equalize the Early-Late correlator (E-L) values in tracking, it fails to track the LOS signal code phase correctly due to the ACF deformation from MP. Notice that the LOS peak, denoted by the red line in Fig. 3 is not aligned with the prompt correlator, which denotes the estimated LOS code phase by tracking i.e., zero mark of  $\Delta\phi$ . This difference is the pseudorange error from MP, and since 2SP uses this MP-affected pseudorange in its PVT computation, the error is propagated into the PVT estimation. On the contrary, DPE is *in theory* immune to the effects of both constructive and destructive MP if the relative signal amplitude of the reflected signal is lower than the LOS (Bialer et al. 2013).

Under the assumption that the reflected path is weaker than the LOS, the peak of the ACF still corresponds to the LOS peak i.e., the peak of the ACF still corresponds to the correct LOS code delay or pseudorange value. Thus, the highest correlation value is still given to candidate PVTs with the true range. Empirically, this also applies to destructive MP cases. But for a constructive MP, notice from Fig. 3 that the right-hand part of the ACF is elevated due to the constructive interference of the reflected signal with the LOS. With the effects of noise, the ACF peak may not correspond to the LOS peak in real cases. Xie and Petovello (2015) had also previously discovered that the ACF peak does not necessarily correspond to the LOS peak in real urban environments i.e., a stronger reflected signal than the LOS. In this case, DPE signal model will be misspecified as the assumption for the LOS peak being the highest in (1) becomes invalid, leading to poor performance from DPE (Bialer et al. 2013). A worst-case scenario of the ACF deformation in real urban environments is shown in Fig. 4 below.



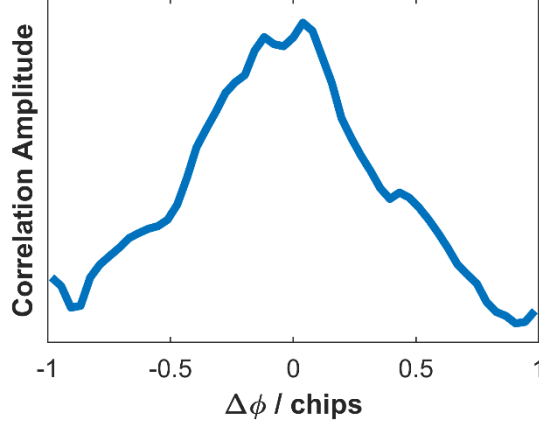


**Fig. 4** An example of an ACF from real urban data.

In addition, even simulated cases of MP have been shown to induce errors of tens of meters to DPE (Tang et al. 2024). Indeed, DPE remains robust against 2SP, but since wide range of research has investigated ways to reduce MP errors for 2SP, the prevalence of DPE as a robust positioning algorithm has been strongly diminished. As a result, an MMT-integrated DPE is proposed.

### Multipath Mitigation Technology

Weill (2002) introduced MMT as a more computationally efficient alternative to his previously introduced MP estimating algorithm, the Minimum Mean-Square Error (MMSE), which required a six-fold integration to produce the delay estimates of the LOS path. Assuming a single-path MP reception, for a Doppler-compensated and navigation data free signal, the received baseband signal in equation (2), sampled at time  $t$ , can be simplified as the following

$$x(t) = a^{\text{LOS}} \cdot m^{\text{LOS}}\{t - \tau^{\text{LOS}}\} \cdot e^{j\varphi_{\text{carr},t}^{\text{LOS}}} + a^{\text{NLOS}} \cdot m^{\text{NLOS}}\{t - \tau^{\text{NLOS}}\} \cdot e^{j\varphi_{\text{carr},t}^{\text{NLOS}}} + n(t) \quad (5)$$

where  $m\{\cdot\}$  represents the ranging code.  $\tau^{\text{LOS}}$  and  $\tau^{\text{NLOS}}$  represent the code delay of the LOS and reflected or NLOS path respectively (Weill 2002).  $\varphi_{\text{carr},t}^{\text{LOS}}$  and  $\varphi_{\text{carr},t}^{\text{NLOS}}$  represents the carrier phase of the LOS and reflected or NLOS path respectively.  $a^{\text{LOS}}$  and  $a^{\text{NLOS}}$  represents the amplitude of the LOS and reflected or NLOS path respectively. Separating the in-phase (Real) and quadrature (Imaginary) components yields

$$x_{\text{Real}}(t) = a^{\text{LOS}} \cdot m^{\text{LOS}}\{t - \tau^{\text{LOS}}\} \cdot \cos(\varphi_{\text{carr},t}^{\text{LOS}}) + a^{\text{NLOS}} \cdot m^{\text{NLOS}}\{t - \tau^{\text{NLOS}}\} \cdot \cos(\varphi_{\text{carr},t}^{\text{NLOS}}) + n_{\text{Real}}(t) \quad (6)$$

$$x_{\text{Imaginary}}(t) = a^{\text{LOS}} \cdot m^{\text{LOS}}\{t - \tau^{\text{LOS}}\} \cdot \sin(\varphi_{\text{carr},t}^{\text{LOS}}) + a^{\text{NLOS}} \cdot m^{\text{NLOS}}\{t - \tau^{\text{NLOS}}\} \cdot \sin(\varphi_{\text{carr},t}^{\text{NLOS}}) + n_{\text{Imaginary}}(t) \quad (7)$$

where  $n_{\text{Real}}(t)$  and  $n_{\text{Imaginary}}(t)$  represent noise in the real and imaginary components respectively, both independent, real-valued, and follows AWGN. To estimate the MP parameters, MMT involves the minimization of the following cost function (Weill 2002).

$$\Gamma = \int_0^T \left[ \begin{array}{c} x_{\text{Real}}(t) - a^{\text{LOS}} \cdot m^{\text{LOS}}\{t - \tau^{\text{LOS}}\} \cdot \cos(\varphi_{\text{carr},t}^{\text{LOS}}) \\ -a^{\text{NLOS}} \cdot m^{\text{NLOS}}\{t - \tau^{\text{NLOS}}\} \cdot \cos(\varphi_{\text{carr},t}^{\text{NLOS}}) \end{array} \right]^2 dt + \int_0^T \left[ \begin{array}{c} x_{\text{Imaginary}}(t) - a^{\text{LOS}} \cdot m^{\text{LOS}}\{t - \tau^{\text{LOS}}\} \cdot \sin(\varphi_{\text{carr},t}^{\text{LOS}}) \\ -a^{\text{NLOS}} \cdot m^{\text{NLOS}}\{t - \tau^{\text{NLOS}}\} \cdot \sin(\varphi_{\text{carr},t}^{\text{NLOS}}) \end{array} \right]^2 dt \quad (8)$$

where  $T$  is the end of the sampling window.  $\Gamma$  typically involves a non-linear optimization with six-parameter search space consisting of  $\tau^{\text{LOS}}$ ,  $\tau^{\text{NLOS}}$ ,  $\varphi_{\text{carr},t}^{\text{LOS}}$ ,  $\varphi_{\text{carr},t}^{\text{NLOS}}$ ,  $a^{\text{LOS}}$ , and  $a^{\text{NLOS}}$ . But instead, Weill (2002) used the following invertible transformation

$$A = a^{\text{LOS}} \cdot \cos(\varphi_{\text{carr},t}^{\text{LOS}}) \quad B = a^{\text{LOS}} \cdot \sin(\varphi_{\text{carr},t}^{\text{LOS}})$$

$$C = a^{\text{NLOS}} \cdot \cos(\varphi_{\text{carr},t}^{\text{NLOS}}) \quad D = a^{\text{NLOS}} \cdot \sin(\varphi_{\text{carr},t}^{\text{NLOS}}) \quad (9)$$

which transforms (8) into

$$\Gamma = \int_0^T [x_{\text{Real}}^2(t) + x_{\text{Imaginary}}^2(t)] dt + (A^2 + B^2 + C^2 + D^2) \cdot R_{\text{mm}}(0) - 2 \cdot A \cdot R_{\text{Real},m}(\tau^{\text{LOS}}) - 2 \cdot B \cdot R_{\text{Real},m}(\tau^{\text{NLOS}}) + 2 \cdot A \cdot B \cdot R_{\text{mm}}(\tau^{\text{LOS}} - \tau^{\text{NLOS}}) - 2 \cdot C \cdot R_{\text{Imag},m}(\tau^{\text{LOS}}) - 2 \cdot D \cdot R_{\text{Imag},m}(\tau^{\text{NLOS}}) + 2 \cdot C \cdot D \cdot R_{\text{mm}}(\tau^{\text{LOS}} - \tau^{\text{NLOS}}) \quad (10)$$

where  $R_{\text{mm}}$  is the autocorrelation function between two local replicas,  $R_{\text{Real},m}$  and  $R_{\text{Imag},m}$  are the cross-correlation between the local code replicas with (6) and (7) respectively (Chen et al. 2013). This ingenious transformation allows the original six-dimensional problem of (8) to turn into a two-dimensional optimization, through the minimization of (10) with respect to  $A$ ,  $B$ ,  $C$ , and  $D$ . Said minimization can be achieved by taking the partial derivatives of (10) with respect to said parameters

$$\frac{\partial \Gamma}{\partial A} = 2 \cdot A \cdot R_{\text{mm}}(0) - R_{\text{Real},m}(\tau^{\text{LOS}}) + 2 \cdot B \cdot R_{\text{mm}}(\tau^{\text{LOS}} - \tau^{\text{NLOS}}) = 0$$

$$\frac{\partial \Gamma}{\partial B} = 2 \cdot B \cdot R_{\text{mm}}(0) - R_{\text{Real},m}(\tau^{\text{NLOS}}) + 2 \cdot A \cdot R_{\text{mm}}(\tau^{\text{LOS}} - \tau^{\text{NLOS}}) = 0$$

$$\frac{\partial \Gamma}{\partial C} = 2 \cdot C \cdot R_{\text{mm}}(0) - R_{\text{Imag},m}(\tau^{\text{LOS}}) + 2 \cdot D \cdot R_{\text{mm}}(\tau^{\text{LOS}} - \tau^{\text{NLOS}}) = 0$$

$$\frac{\partial \Gamma}{\partial D} = 2 \cdot D \cdot R_{\text{mm}}(0) - R_{\text{Imag},m}(\tau^{\text{NLOS}}) + 2 \cdot C \cdot R_{\text{mm}}(\tau^{\text{LOS}} - \tau^{\text{NLOS}}) = 0 \quad (11)$$

For each potential (candidate) values of  $\tau^{\text{LOS}}$  and  $\tau^{\text{NLOS}}$ , (11) allows the computation of their corresponding  $A$ ,  $B$ ,  $C$ , and  $D$ , which together with  $\tau^{\text{LOS}}$  and  $\tau^{\text{NLOS}}$  acts as inputs for (10). Our implementation of MMT uses the grid-based method, in which a grid of  $\tau^{\text{LOS}}$  and  $\tau^{\text{NLOS}}$  pairs of 0.005 chips spacing are first generated and the pair of  $\tau^{\text{LOS}}$  and  $\tau^{\text{NLOS}}$  which minimizes (10) will be MMT's estimate of the LOS and NLOS delays. Since  $\tau^{\text{NLOS}}$  is always be larger than  $\tau^{\text{LOS}}$ , pair delays with  $\tau^{\text{NLOS}}$  smaller than the  $\tau^{\text{LOS}}$  is not considered (Blanco-Delgado and Nunes 2012). To improve the performance of MMT, the following constraint is used on the amplitudes, in the form of a Lagrange multiplier (Weill 2002).

$$\frac{a^{\text{NLOS}}}{a^{\text{LOS}}} \leq 0.8 \quad (12)$$

### Proposed MMT-integrated DPE

The proposed MMT-integrated DPE methodology aims to solve DPE misspecified signal model due to MP from a practical standpoint, by associating the highest ACF peak (from the pre-calculated correlations) with  $\tau^{\text{LOS}}$  estimated by an MMT. In other words, the zero mark of  $\Delta\phi$  in Fig. 3 will directly be aligned with the ACF peak (the red line). This practically solves the misspecified signal model of DPE since in DPE signal model, the highest correlation value of a satellite should correspond to  $\tau^{\text{LOS}}$ . Since the proposed DPE uses 2SP tracking to propagate the channel, MMT is implemented to 2SP tracking i.e., an MMT-aided tracking.

The MMT-integrated DPE (and MMT-integrated 2SP) uses *tracking MMT.m* instead of *tracking.m* as shown in Fig. 1. Though MMT is integrated to DPE at 2SP tracking, the proposed MMT-integrated DPE should also be applicable to snapshot DPE methodologies, such as that from Axelrad et al. (2009, 2011) and Tang et al. (2024).

The discriminator output in 2SP tracking, in which the SoftGNSS is configured to use the normalized Early-minus-Late power discriminator, will directly be replaced with  $\tau^{\text{LOS}}$  estimates from MMT. This automatically leads to MP-free pseudorange estimates for 2SP, which will also later be used by *DPE\_module.m* for positioning. Since the MMT architecture uses the grid-based method, the computation of MMT is done with the parallel pool (*parfor*) function from MATLAB's parallel computing toolbox to accelerate MMT computation.

Since DPE signal model assumes that the highest ACF peak corresponds to the LOS peak, associating the ACF peak to an MMT-corrected pseudorange i.e.,  $\tau^{\text{LOS}}$  allows the highest correlation value to be given to candidate PVTs with the true range. A benefit of using MMT is that it can still manage to estimate  $\tau^{\text{LOS}}$  correctly even if the relative amplitude of the reflected signal is larger than 1 (Chen et al. 2013).

In this case, if the MP reception has been compensated for both DPE and 2SP, and because both positioning methods use  $\tau^{\text{LOS}}$  from MMT, both should have similar positioning performance in MP-only environments. While DPE is not supposed to involve the estimation of the code delays, the proposed MMT-integrated DPE can be said to still be considered as *DPE* since

1. It still solves the PVT directly in the navigation domain.

2. Uses real signal correlations.
3. The LOS code delay i.e., MMT-corrected pseudoranges, corresponds to the highest ACF peak, fulfilling DPE signal model. The reason for not involving the estimation of pseudoranges in DPE is due to the loss of precision of pseudorange estimation, and that it would be MP error-affected. Now that the pseudoranges are compensated for MP and precise from MMT, it is valid to use it to aid DPE.

Indeed, the proposed MMT-integrated DPE deviates from the previously introduced DPE architectures, since it requires estimation of since the MMT  $\tau^{\text{LOS}}$  estimates. Thus, the MMT-integrated DPE is proposed as a variant of DPE instead, one that is designed to be more suitable for urban environment applications, which will later be shown in the results.

Since the proposed MMT-integrated DPE uses pseudorange observables that are byproducts of tracking, its performance against weak signals reception degrades consequently. But under sufficiently large number of satellites available, the use of real signal correlations can still benefit the MMT-integrated DPE since the weak signals are automatically weighted down during positioning as it has weaker signal correlations.

## Data Collection Method

Evaluation of the proposed DPE module will use both real and simulated static GNSS data. Three front-ends were involved in collection of real data; National Instruments Universal Software Radio Peripheral (NI USRP) B210, NI USRP N210, and NSL Stereo.

For the NI USRP front-ends, a ZYACF-L004 antenna was used, powered by a bias-tee. The NI USRP was connected to an Ubuntu laptop with GNU Radio to record and save the down-converted IF data. For the NI USRP B210, a sampling frequency of 20 MHz was used, with bandwidth of 2 MHz. Conversely, the NI USRP N210 used a wider 10 MHz bandwidth with a sampling frequency of 10 MHz. For the N210, since it does not draw power from the laptop like the B210, a battery pack was required to power it. This battery pack was also used to power the bias-tee. On the other hand, datasets collected with the NSL Stereo used an Allystar AGR6303 antenna. The NSL Stereo has a 26 MHz sampling frequency and an 8 MHz bandwidth (Xu et al. 2019a). For the simulated urban datasets, a Spirent simulator was used to generate datasets with known MP and NLOS parameters. The simulator was connected to a LabSat 3W front-end, configured with 58 MHz of sampling frequency and 56 MHz of front-end bandwidth. Ground truth for all the collected urban datasets were taken with a u-Blox F9P receiver, which uses a multi-constellation Real-Time Kinematic (RTK) positioning to obtain centimeter-level accuracy.

## Results and Discussion

The results section will first investigate the performance of pure DPE and 2SP. 2SP scalar tracking is configured to use 0.6 E-L chip spacing for all of the results. In cases with no MP or NLOS, both 2SP and DPE are expected to have comparable positioning performance (Closas and Gusi-Amigó 2017). Real open-sky BeiDou B1I data was collected from the roof of R-core building of The Hong Kong Polytechnic University

to illustrate the case. Fig. 5 shows the skymask as well as the positioning result from both DPE and 2SP.

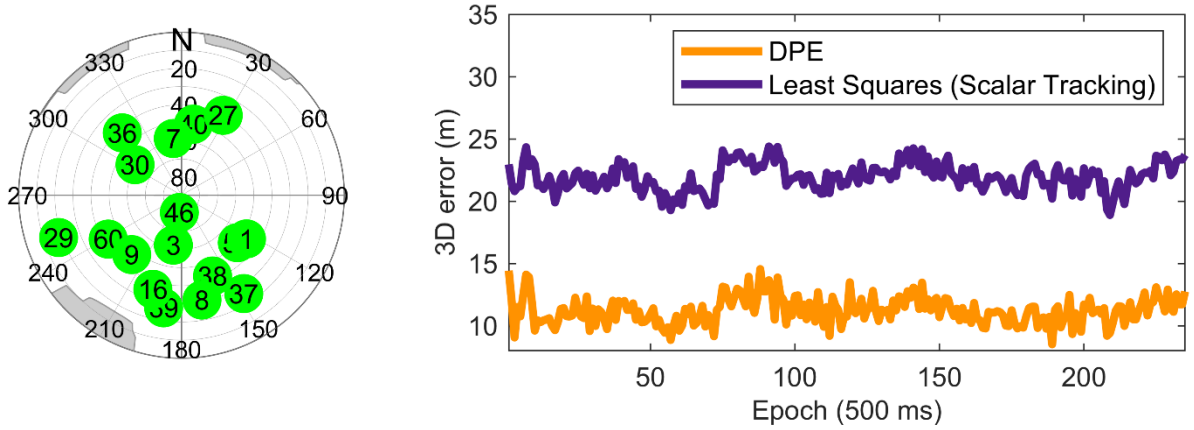


**Fig. 5** Positioning results from DPE and 2SP with BeiDou B1I open-sky dataset, with an average 3D mean error of 21.94 meters and 11.23 meters from 2SP and DPE, respectively. This dataset was collected with the NI USRP N210.

Even though collected in an open-sky environment, the fluctuation in the positioning error from Fig. 5 indicates the existence of MP, making it more of a light urban environment instead of open-sky. The result from Fig. 5 clearly favors DPE, due to its inherent MP mitigation property. Similar results can be observed with a GPS L1 C/A open-sky dataset. Fig. 6 shows the open-sky results with GPS L1 C/A.

Evaluating DPE under controlled environments, a Spirent simulator was used to generate two simulated urban conditions; medium urban and harsh urban. In the simulated light urban environment, there are a total of 8 GPS L1 C/A satellites, with one simulated constructive MP satellite of 0.1 chip relative delay (and 0.5 relative amplitude) for the reflected signal and one NLOS satellite with 0.2 chip additional delay. Fig. 7 presents the positioning result for the simulated light urban dataset.

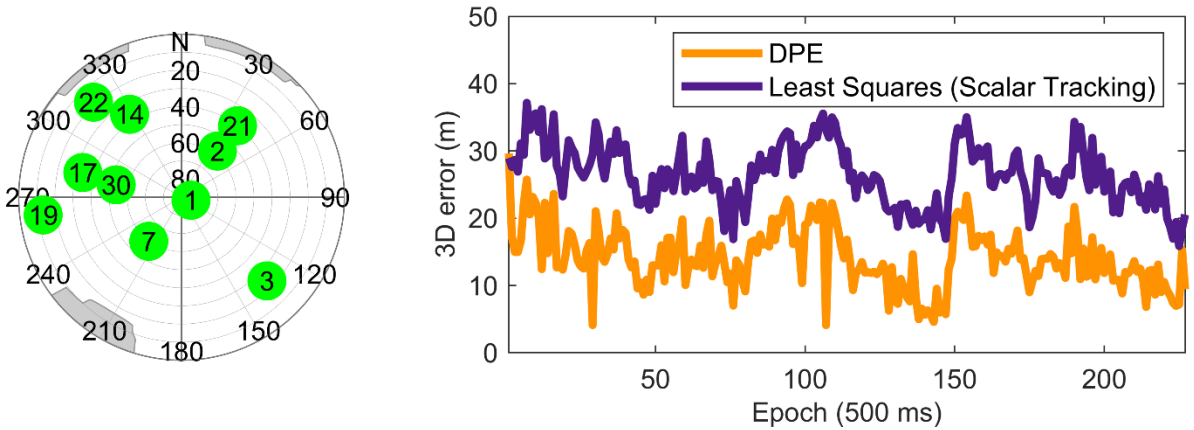


**Fig. 6** Positioning results from DPE and 2SP with GPS L1 C/A open-sky dataset, with an average 3D mean error of 26.51 meters and 14.16 meters from 2SP and DPE, respectively. This dataset was collected with the NI USRP N210.

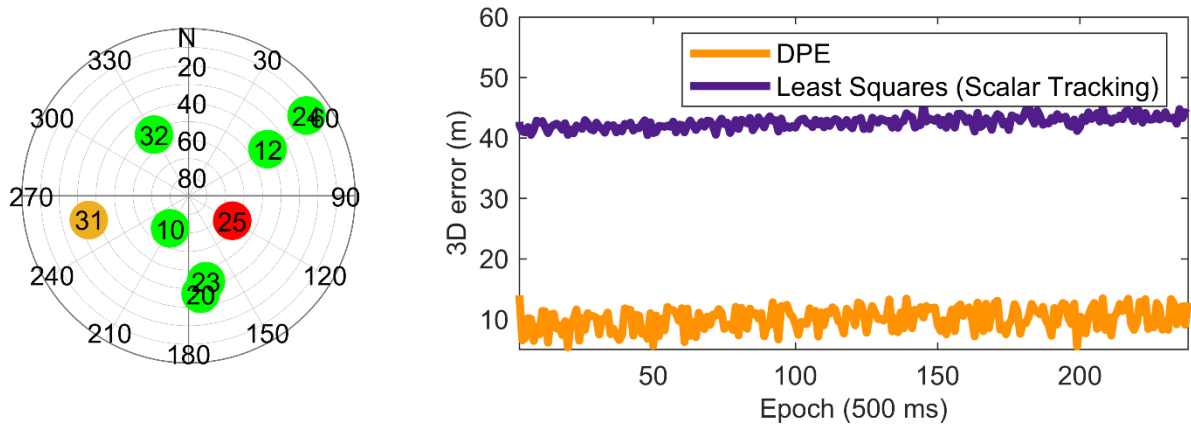


**Fig. 7** Positioning results from DPE and 2SP under a simulated GPS L1 C/A medium urban condition, with an average 3D mean error of 42.98 meters and 10.40 meters from 2SP and DPE, respectively. PRN 25 (highlighted in red) is the simulated NLOS satellite, while PRN 31 (highlighted in orange) is the simulated MP.

On the contrary, there are a total of 9 GPS L1 C/A satellites for the simulated harsh urban dataset. Three satellites are constructive MP, with PRN12 configured to have 0.05 chip relative delay (and 0.8 relative amplitude), PRN 6 with 0.1 chip relative delay (and 0.5 relative amplitude), and PRN23 with 0.3 chip relative delay (and 0.4 relative amplitude) for the reflected signal. A single NLOS satellite was also simulated, configured with 0.3 chip of additional delay. The results are elaborated in Fig. 8. Results from the Spirent simulated datasets clearly show DPE positioning robustness in comparison to 2SP, with 75.81% mean outperformance with the simulated medium urban dataset. But for the harsh urban, the geometry of the MP and NLOS satellites allows for the pseudorange errors to cancel out, leading to similar performance from 2SP and DPE.

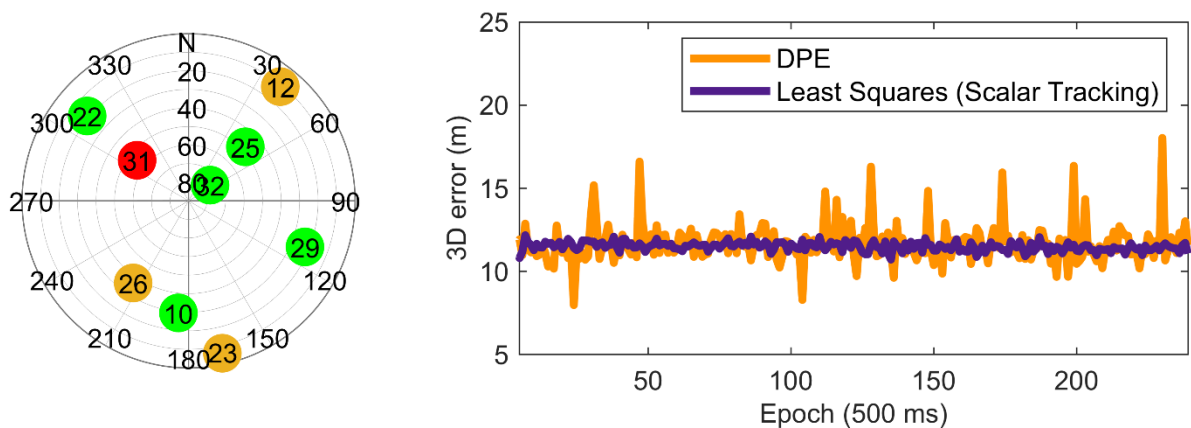


**Fig. 8** Positioning results from DPE and 2SP under a simulated GPS L1 C/A harsh urban condition, with an average 3D mean error of 12.08 meters and 11.79 meters from 2SP and DPE, respectively. PRN 31 (highlighted in red) is the simulated NLOS satellite, while PRN 12, 23 and 26 (highlighted in orange) are the simulated MP satellites.

While previously, the resilience of GNSS DPE against MP has been thoroughly established, it is revealed that it has strong resilience against NLOS as well, supporting the arguments on Direct Position Determination (DPD) (Amar and Weiss 2005; Bialer et al. 2013). The findings from the simulated datasets are further supported by real GPS

L1 C/A data with one NLOS satellite. Fig. 9 provides the result from a GPS L1 C/A medium urban dataset collected in East Tsim Sha Tsui, close to The Hong Kong Polytechnic University. With PRN 22 blocked by a nearby building (denoting NLOS reception), DPE manages to offer a 36.48% improvement in mean error compared to 2SP.

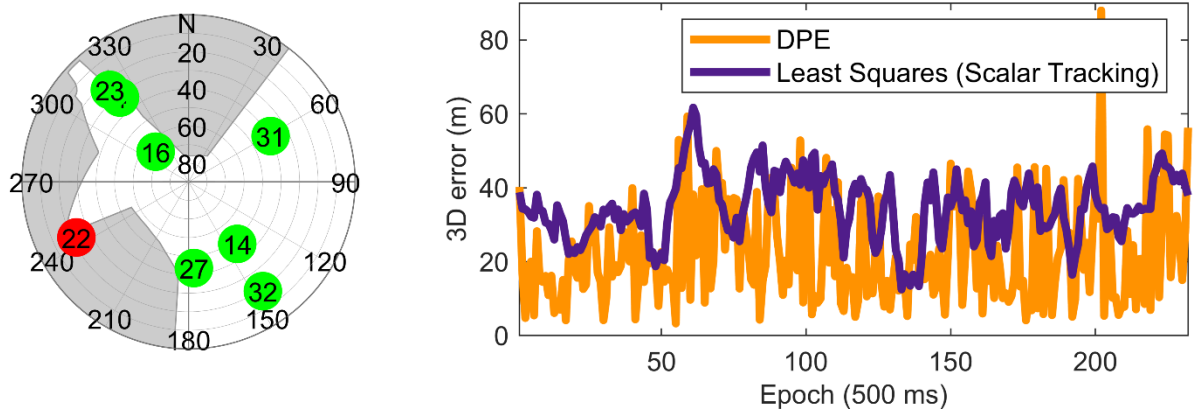


**Fig. 9** Positioning results from DPE and 2SP from a medium urban GPS L1 C/A dataset collected in East Tsim Sha Tsui, with an average 3D mean error of 34.75 meters and 22.07 meters from 2SP and DPE, respectively. PRN 22 (highlighted in red) is the NLOS satellite. This dataset was collected with NSL Stereo.

The research findings on DPE resilience against NLOS also concurs with the author’s previous findings on an DPE-based positioning scheme, in which it solving the PVT in the navigation domain is crucial for NLOS resilience as it allows the exclusion of the error-affected satellite measurements from contributing to the final PVT (Vicenzo et al. 2024).

The case can be further illustrated by digging deeper into the correlograms result for an NLOS satellite. Fig. 10 shows the comparison between the correlograms of a high-elevated satellite and NLOS satellite from the medium urban dataset in Fig. 9. Fig. 10 clearly illustrates how the correlations of an NLOS satellite deviate from the ground truth. And in contrast, for a high-elevated satellite (which for the sake of argument, is assumed to be LOS), the correlations converge to the ground truth. On top of that, Fig. 10 clearly shows that the correlations of an NLOS satellite are much weaker compared to that of the highly elevated, which inherently gives a lower weighting to the NLOS satellite during the PVT estimation.

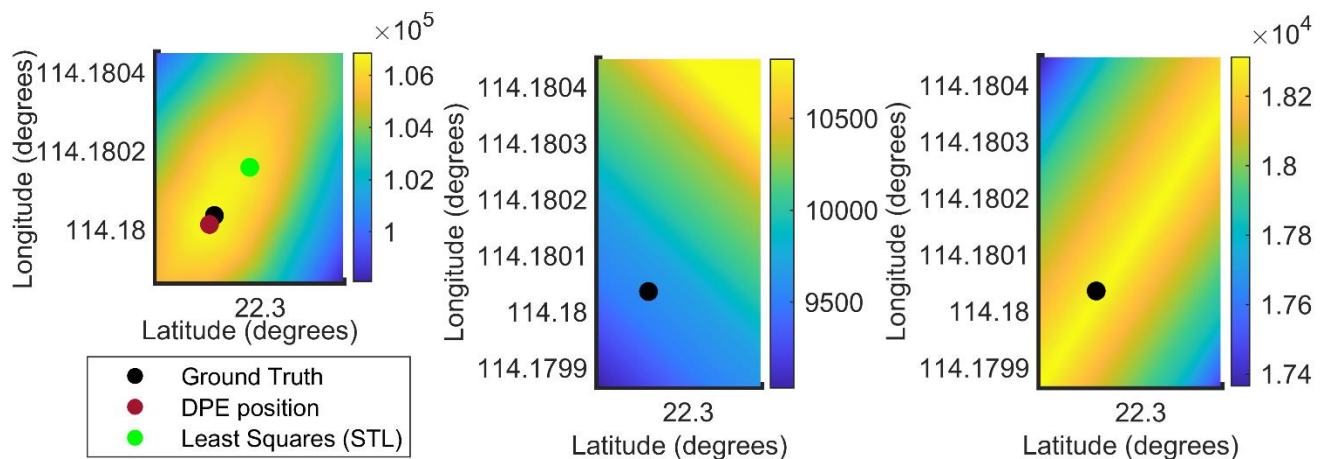


**Fig. 10** Correlogram of an NLOS satellite, PRN 22 (Center) in Fig. 9 and that of a highly elevated satellite, PRN 16 (Right) in Fig. 9. The final correlogram after summing up individual satellite correlations (Left) shows the position estimate from DPE remains close to the ground truth unlike 2SP.

Hence, NLOS satellite correlations do not contribute to the global maxima or in other words, its measurements are excluded from the final PVT estimation of DPE, and that final DPE PVT estimate made use of the correlations from the other satellites in view (Vicenzo et al. 2023; Amar and Weiss 2005; Bialer et al. 2013).

Tang et al. (2024) had presented that DPE manages to obtain much more accurate positioning even if the majority of signals received are MP. For the sake of completion, Fig. 11 illustrates the positioning error from the harsh urban Spirent data when only PRN 22, 12, 23, and 26 are left i.e., 3 MP signals and 1 LOS. Except for a few outliers, DPE manages to consistently obtain a much more accurate position in comparison to 2SP, highlighting that the proposed DPE implementation meets the expected theoretical DPE MP mitigation capability previously elaborated above.

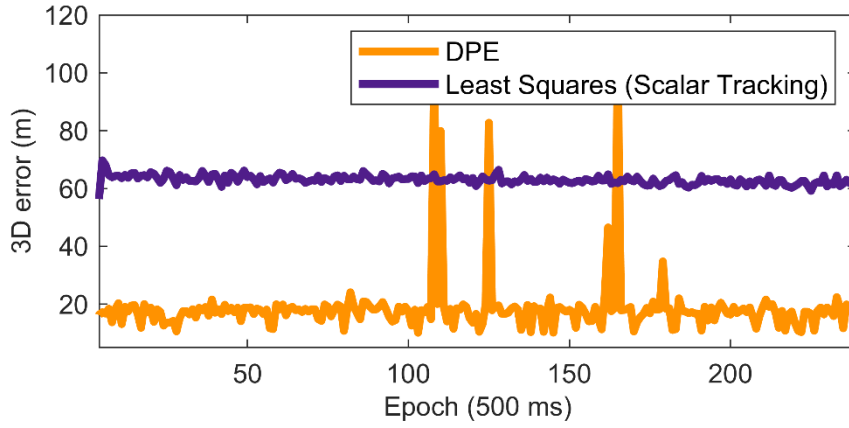


**Fig. 11** Positioning results from DPE and 2SP when there is only a single LOS satellite and 3 MP satellite i.e., an extremely harsh urban case, with an average 3D mean error of 63.68 meters and 18.95 meters from 2SP and DPE, respectively.

Moving into the results of the MMT-integrated DPE, the performance of MMT estimates is first analysed with the harsh urban Spirent data. Since the  $\tau^{\text{LOS}}$  estimates from MMT are used to replace the normalized Early-minus-Late power discriminator output in tracking, the discriminator output is compared to the  $\tau^{\text{LOS}}$  from MMT in Fig. 12. Fig. 12 clearly shows that  $\tau^{\text{LOS}}$  from MMT has a much lower variance in 2SP tracking error compared to the discriminator.



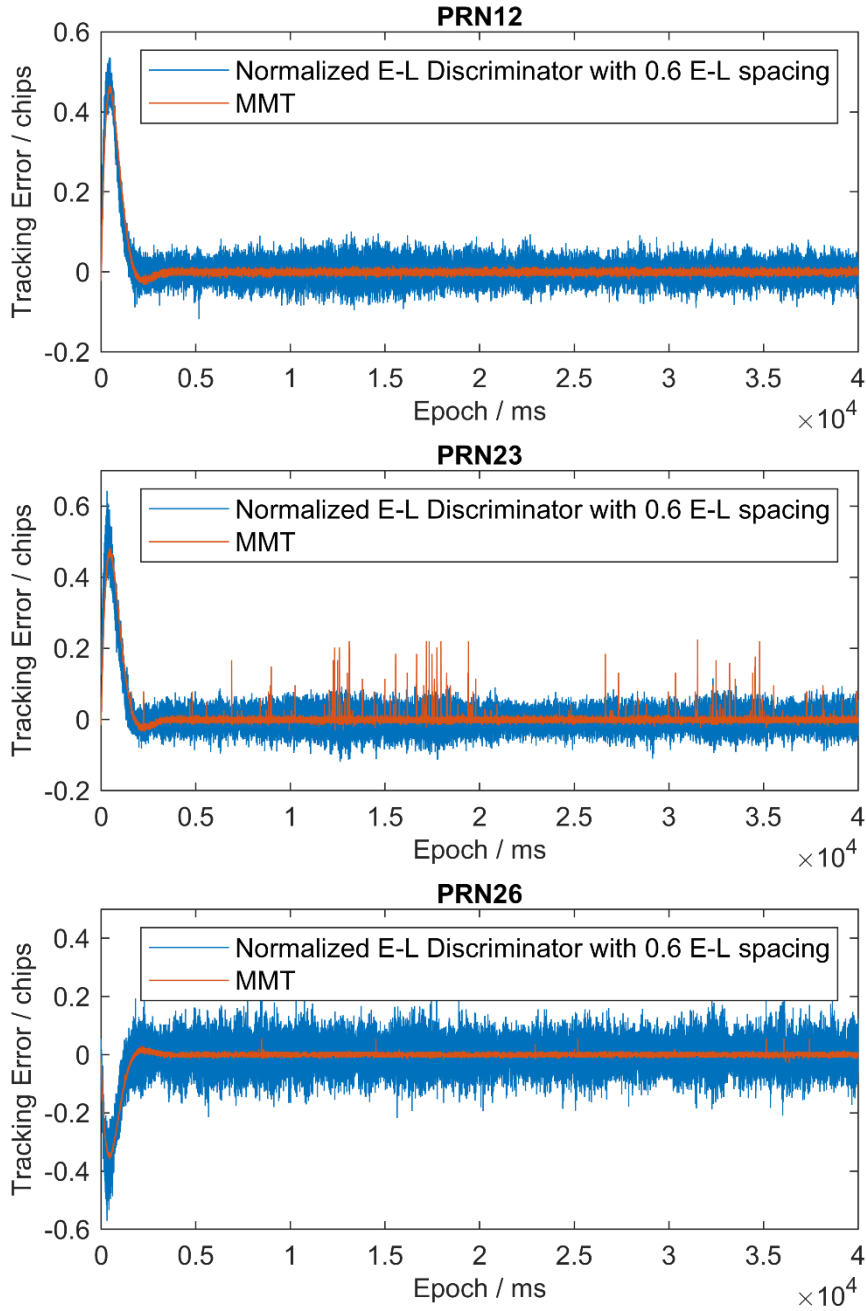


**Fig. 12** Comparison of normalized Early-minus-Late power discriminator output with the  $\tau^{\text{LOS}}$  from MMT when integrated into 2SP tracking.

The effect of using MMT will directly be investigated under the extremely harsh simulated condition from Fig. 11 i.e., four satellites with three being MP (PRN12, 23, and 26) and one LOS (PRN22). The positioning result is elaborated on Fig. 13 below. Ignoring the first several seconds from the tracking loops to stabilize, both MMT-integrated DPE and MMT-integrated 2SP manages to obtain similar positioning results, with DPE 3D error to be 11.30 meters and 2SP being 11.16 meters. This presents not only a huge improvement for 2SP, which originally has a mean 3D error of 63.68 meters, but also for DPE, which originally has a mean error of 18.95 meters.

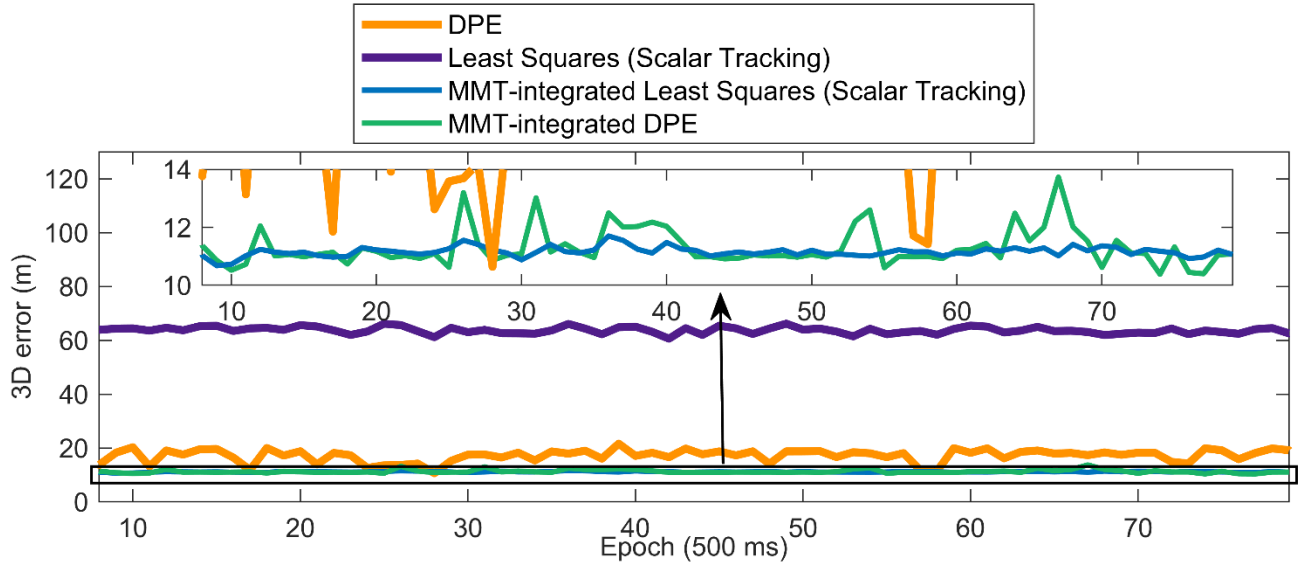


**Fig. 13** Comparison of positioning results from MMT-integrated DPE and 2SP with pure DPE and 2SP when there is only a single LOS satellite and 3 MP satellite.

It must be reminded that even though both 2SP and DPE now performs similarly now that the MP reception is taken into account into the signal models, NLOS reception is also prominent in urban environments, which cannot be compensated with MMT for both DPE and 2SP. But as illustrated above, the inherent superiority of DPE to NLOS allows the MMT-integrated DPE positioning to remain accurate when NLOS is introduced. To illustrate this case, the positioning results of the original Spirent harsh urban dataset with 9 satellites and a single NLOS of 0.3 chips relative delay with MMT-integrated DPE and 2SP is shown on Fig. 14.

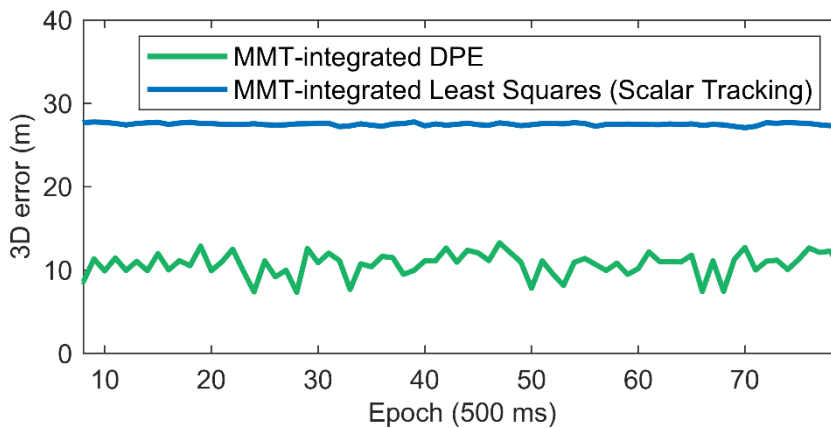


**Fig. 14** Positioning results from MMT-integrated DPE and 2SP under a simulated GPS L1 C/A harsh urban condition, with an average 3D mean error of 27.51 meters and 10.70 meters from 2SP and DPE, respectively.

With this dataset, both DPE and 2SP originally performed similarly, as shown in Fig. 8 due to the geometry of the error-affected satellites allowing the pseudorange errors to cancel each other out for 2SP. But now that the MP is compensated, the error only originates from the NLOS satellite, which based on Fig. 14, increases the error for 2SP. On the contrary, since the NLOS satellite correlations is deviated away from the ground truth, the MMT-integrated DPE manages to harness the other LOS and MP-compensated satellite measurements to produce a much more accurate global maxima in the navigation domain, which consequently makes it immune to the NLOS satellite.

Further proving the robustness of the proposed MMT-integrated DPE, the results with real data from Fig. 9, which has a single NLOS satellite, is shown in Fig. 15. The original DPE outperformance of 36.48% against pure 2SP is now increased to 49.75%, with MMT-integrated DPE has a mean 3D error of 17.46 meters while 2SP is 32.19 meters, thus proving that the MMT-integrated DPE is the more suitable option for urban positioning in comparison to pure DPE, pure 2SP, and MMT-integrated 2SP.

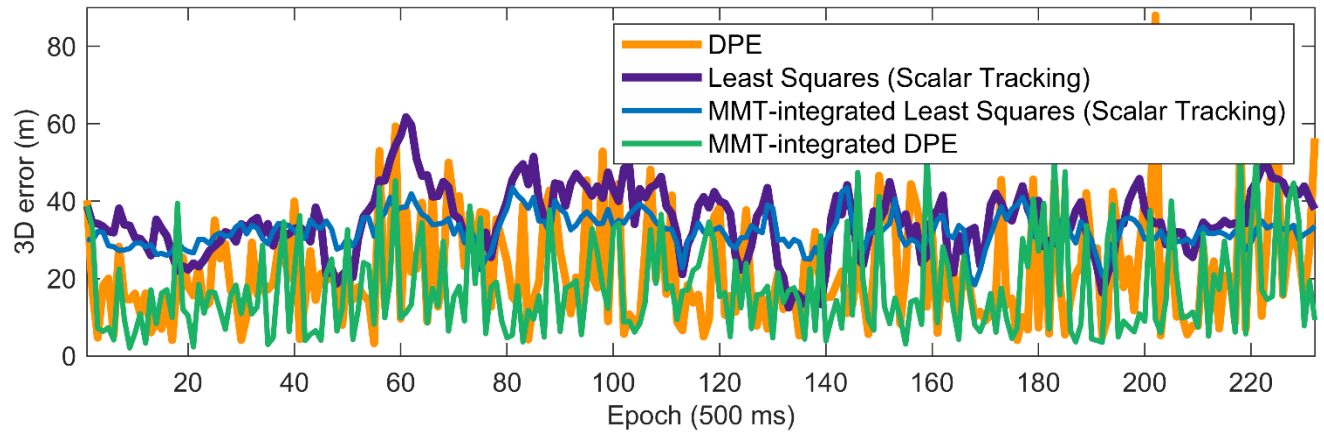


**Fig. 15** Positioning results from DPE and 2SP from a medium urban GPS L1 C/A dataset collected in East Tsim Sha Tsui, a single NLOS satellite.

A disclaimer, the proposed DPE module seems to falter greatly against 2SP when tested in urban environments with a front-end bandwidth of 2 MHz. This is due to the flattening of the top of the ACF due to the narrow front-end bandwidth which increases the ambiguity of the correlations in the navigation domain. An example is illustrated with a medium urban dataset was collected at The Hong Kong Polytechnic University. Fig. 16 shows the result from a medium urban dataset collected in front of the Stanley Ho building of The Hong Kong Polytechnic University campus. To that end, analysis of the proposed DPE module has been focused on using IF data with front-ends bandwidths of 8 MHz and larger. Considering that current GNSS receivers must accommodate multiple frequency bands from various GNSS constellations to permit multi-constellation positioning, bandwidths larger than 8 MHz is a reasonable configuration for SDRs.

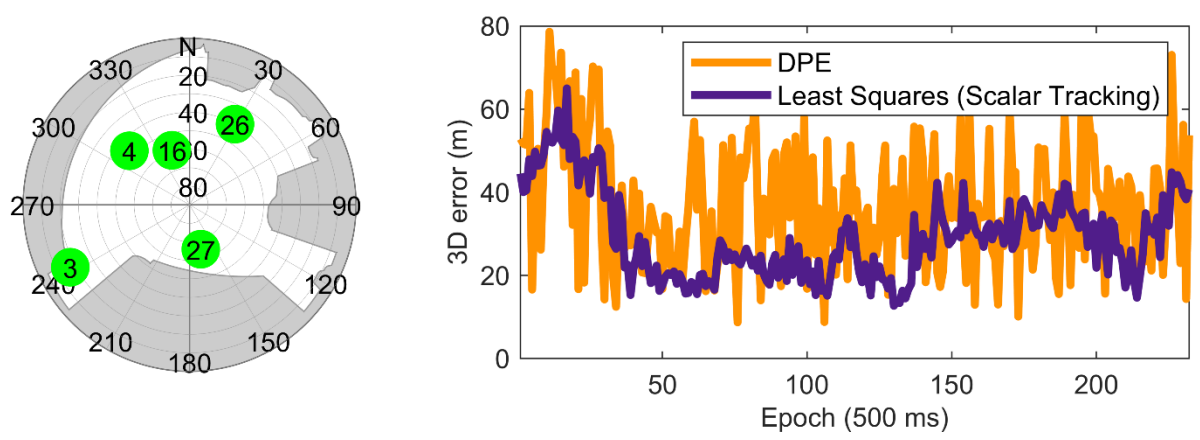


**Fig. 16** Positioning results from DPE and 2SP from a GPS L1 C/A medium urban dataset collected in The Hong Kong Polytechnic University campus. This dataset was collected with NI USRP B210, which has a front-end bandwidth of 2 MHz.

## Conclusion

We have presented a novel implementation of a DPE receiver, which has been made open-sourced to the GNSS community through the GitHub page <https://github.com/Sergio-Vicenzo/GPSL1-DPEmodule>. With the aim of better familiarization and understanding of DPE, the proposed DPE is programmed in the user-friendly and easy-to-learn programming language, MATLAB and as a module that can be integrated into existing MATLAB 2SP SDRs. Currently, the DPE module is made open source integrated into the SoftGNSS MATLAB GPS L1 C/A 2SP SDR from Borre et al. (2007), which is based on STL. But integration of the proposed DPE module is not restricted to an STL-based receiver and can be integrated with other 2SP architectures, such as VTL. Additionally, the GNSS constellation is also not restricted to GPS L1 C/A, but is also integrable with SDRs working with other BPSK-modulated GNSS signals. The results section has shown results from using BeiDou B1I signal, which has a similar signal structure with GPS L1 C/A.

Results clearly prove that the proposed DPE plug-in module still harnesses the established advantages of DPE and consistently outperforms 2SP in the tested real and simulated datasets. DPE manages to achieve 75.81% positioning improvement in a simulated medium urban and 36.48% for real medium urban. Even when three out of four satellites are MP i.e., an extremely harsh urban case, DPE manages to maintain an average error below 20 meters whereas 2SP error goes beyond 60 meters.

A variant of DPE, dubbed MMT-integrated DPE has also been introduced to improve DPE resilience against MP, which has also been made available at the GitHub page <https://github.com/Sergio-Vicenzo/GPSL1-MMT-DPEmodule>. Though DPE manages to consistently achieve lower positioning errors compared to 2SP, recent research has shown that under severe MP conditions, its error can still explode to tens of meters like 2SP does. As a result, MMT-integrated DPE was introduced to better suit DPE for applications in urban environments. Under MP-only conditions, both MMT-integrated DPE and 2SP perform similarly. But since DPE also has a natural NLOS mitigation property, MMT-integrated DPE consistently outperforms MMT-integrated 2SP when both MP and NLOS exist. Under a harsh urban simulated data with both MP and NLOS, the MMT-integrated DPE manages to maintain the same error as without NLOS, which further highlights its NLOS mitigation property. In contrast, the MMT-integrated 2SP error increases to a large degree compared to unaided 2SP since the errors from MP are eliminated, which results in the MP errors to no longer cancel out with NLOS from the effect of geometry.

The results from real urban data with NLOS supports the results from the simulated data. While an MMT-integrated 2SP seems to not significantly improve 2SP positioning, due to the existence of NLOS, the MMT-integrated DPE manages to further outperform both MMT-integrated 2SP and unaided 2SP by up to 49%, making it the preferable choice for urban positioning.

## Declarations

Ethics approval and consent to participate: Not applicable.

Consent for publication: Not applicable.

Availability of data and materials: The proposed open-source DPE plug-in module as well as its MMT derivative is made available by accessing <https://github.com/Sergio-Vicenzo/GPSL1-DPEmodule> as well as <https://github.com/Sergio-Vicenzo/GPSL1-MMT-DPEmodule>

Competing interests: The authors declare that they have no competing interests.

Funding: This study was supported by the National Natural Science Foundation of China (NSFC) under Grant 62103346.

Author contributions: Sergio Vicenzo and Bing Xu developed the idea and methodology. Sergio Vicenzo developed the software. Sergio Vicenzo and Bing Xu conducted formal analysis and investigation. Sergio Vicenzo wrote the main manuscript, conducted the experiment, and prepared the figures and tables. Bing Xu conducted the review, editing and supervision of the work. All authors read and approved the final manuscript.

Acknowledgements: While not directly involved in the research, the authors would like to thank Prof. Dennis M. Akos of the University of Colorado Boulder for his input on having the same coherent and non-coherent integration times for an apple-to-apple comparison between 2SP and DPE during the author's previous presentation in ION GNSS+ 2023. We would also like to thank Dr.-Ing. Jürgen Dampf of Universität der Bundeswehr München, as well as Dr. Pau Closas of the Northeastern University for their valuable suggestions on our DPE implementation at ION GNSS+ 2023.

## References

Amar A, Weiss AJ (2005) Analysis of Direct Position Determination Approach in the Presence of Model Errors. In: Proc. IEEE/SP 13th Workshop on Statistical Signal Processing, IEEE, Bordeaux, France, July 17-20, 1958-1962.

Axelrad P, Bradley BK, Donna J, Mitchell M, Mohiuddin S (2011) Collective Detection and Direct Positioning Using Multiple GNSS Satellites. *Navigation* 58(4):305-321. <https://doi.org/10.1002/j.2161-4296.2011.tb02588.x>

Axelrad P, Donna J, Mitchell M (2009) Enhancing GNSS acquisition by combining signals from multiple channels and satellites. In: Proc. ION GNSS 2009, Institute of Navigation, Savannah, Georgia, USA, September 22 – 25, 3117-3128

Bialer O, Raphaeli D, Weiss AJ (2013) Maximum-Likelihood Direct Position Estimation in Dense Multipath. *IEEE Transactions on Vehicular Technology* 62(5):2069-2079. <https://doi.org/10.1109/TVT.2012.2236895>

Blanco-Delgado N, Nunes FD (2012) Multipath Estimation in Multicorrelator GNSS Receivers using the Maximum Likelihood Principle. *IEEE Transactions on Aerospace and Electronic Systems* 48(4): 3222 - 3233. <https://doi.org/10.1109/TAES.2012.6324696>

- Borre K, Akos DM, Bertelsen N, Rinder P, Jensen SH (2007) A Software-Defined GPS and Galileo Receiver: A Single-Frequency Approach. Birkhäuser, Boston, Massachusetts.
- Cheong JW, Wu J, Dempster AG, Rizos C (2011) Efficient Implementation of Collective Detection. In: Proc. IGNSS Symposium 2011, International Global Navigation Satellite Systems Society, Sydney, New South Wales, Australia, November 15-17.
- Closas P, Fernández -Prades C, Fernández -Rubio JA (2007) Maximum Likelihood Estimation of Position in GNSS. *IEEE Signal Processing Letters* 14(5):359-362. <https://doi.org/10.1109/lsp.2006.888360>
- Closas P, Fernández -Prades C, Fernández -Rubio JA (2009) Cramér–Rao Bound Analysis of Positioning Approaches in GNSS Receivers. *IEEE Transactions on Signal Processing* 57(10):3775-3786. <https://doi.org/10.1109/TSP.2009.2025083>
- Closas P, Fernández-Prades C, Fernández A, Wis M, Vecchione G, Zanier F, Garcia-Molina J, Crisci M (2015) Evaluation of GNSS direct position estimation in realistic multipath channels. In: Proc. ION GNSS+ 2015, Institute of Navigation, Tampa, Florida, USA, September 14 – 18, 3693-3701.
- Closas P, Gao G (2020) Direct Position Estimation. In: Morton YJ, van Diggelen F, Spilker Jr JJ, Parkinson BW, Lo S, Gao G (eds) *Position, Navigation, and Timing Technologies in the 21st Century: Integrated Satellite Navigation, Sensor Systems, and Civil Applications*. Wiley, Hoboken, New Jersey, pp 529-550.
- Closas P, Gusi-Amigó A (2017) Direct Position Estimation of GNSS Receivers: Analyzing main results, architectures, enhancements, and challenges. *IEEE Signal Processing Magazine* 34:72-84. <https://doi.org/10.1109/MSP.2017.2718040>
- Dampf J, Frankl K, Pany T (2018) Optimal Particle Filter Weight for Bayesian Direct Position Estimation in a GNSS Receiver. *Sensors* 18(8):2736. <https://doi.org/10.3390/s18082736>
- Hsu L-T (2018) Analysis and modeling GPS NLOS effect in highly urbanized area. *GPS Solutions* 22(1). <https://doi.org/10.1007/s10291-017-0667-9>
- Li H, Borhani-Darian P, Wu P, Closas P (2022) Deep Neural Network Correlators for GNSS Multipath Mitigation. *IEEE Transactions on Aerospace and Electronic Systems*:1-23. <https://doi.org/10.1109/taes.2022.3197098>
- Li L, Cheong JW, Wu J, Dempster AG (2013) Improvement to Multi-resolution Collective Detection in GNSS Receivers. *Journal of Navigation* 67(2): 277-293. <https://doi.org/10.1017/S0373463313000635>
- Ng H-F, Zhang G, Hsu L-T (2020) A Computation Effective Range-Based 3D Mapping Aided GNSS with NLOS Correction Method. *Journal of Navigation* 73(6):1202-1222. <https://doi.org/10.1017/s037346332000003x>
- Orabi M, Khalife J, Abdallah AA, Kassas ZM, Saab SS (2020) A Machine Learning Approach for GPS Code Phase Estimation in Multipath Environments. In: Proc. IEEE/ION PLANS 2020, Institute of Navigation, Portland, Oregon, USA, April 20 - 23, 1224-1229.

- Peretic M (2019) Development and analysis of a parallelized direct position estimation-based GPS receiver implementation. Thesis, University of Illinois at Urbana-Champaign
- Peretic M, Gao G (2021) Design of a parallelized direct position estimation-based GNSS receiver. *Navigation* 68(1):21-39. <https://doi.org/10.1002/navi.402>
- Phan Q-H, Tan S-L, McLoughlin I (2012) GPS multipath mitigation: a nonlinear regression approach. *GPS Solutions*. <https://doi.org/10.1007/s10291-012-0285-5>
- Tang S, Li H, Calatrava H, Closas P (2023) Precise Direct Position Estimation: Validation Experiments. In: *Proc. IEEE/ION PLANS 2023*, Institute of Navigation, Monterey, California, USA, April 24 - 27, 911-916.
- Tang S, Li H, Closas P (2024) Assessment of Direct Position Estimation Performance in Multipath Channels. In: *Proc. ION GNSS+ 2024*, Institute of Navigation, Baltimore, Maryland, USA, September 16 - 20, 3705 - 3714.
- Vicenzo S, Xu B, Dey A, Hsu L-T (2023) Experimental Investigation of GNSS Direct Position Estimation in Densely Urban Area. In: *Proc. ION GNSS+ 2023*, Institute of Navigation, Denver, Colorado, USA, September 19 – 23, 2906-2919.
- Vicenzo S, Xu B, Xu H, Hsu L-T (2024) GNSS direct position estimation-inspired positioning with pseudorange correlogram for urban navigation. *GPS Solutions* 28(2). <https://doi.org/10.1007/s10291-024-01627-5>
- Weill LR (2002) Multipath Mitigation using Modernized GPS Signals: How Good Can it Get?. In: *Proc. ION GPS 2002*, Institute of Navigation, Portland, Oregon, USA, September 24 - 27, 493 - 505.
- Xie P, Petovello MG (2015) Measuring GNSS Multipath Distributions in Urban Canyon Environments. *IEEE Transactions on Instrumentation and Measurement* 64(2):4604-4619. <https://doi.org/10.1109/TIM.2014.2342452>
- Chen X, Dosis F, Peng S, Yu M (2013) Comparative Studies of GPS Multipath Mitigation Methods Performance. *IEEE Transactions on Aerospace and Electronic Systems* 49(3):1555-1568. <https://doi.org/10.1109/TAES.2013.6558004>
- Xu B, Jia Q, Hsu L-T (2019a) Vector Tracking Loop-Based GNSS NLOS Detection and Correction: Algorithm Design and Performance Analysis. *IEEE Transactions on Instrumentation and Measurement* 69(7):4604-4619. <https://doi.org/10.1109/tim.2019.2950578>
- Xu B, Jia Q, Luo Y, Hsu L-T (2019b) Intelligent GPS L1 LOS/Multipath/NLOS Classifiers Based on Correlator-, RINEX- and NMEA-Level Measurements. *Remote Sensing* 11(16):1851. <https://doi.org/10.3390/rs11161851>
- Xu P, Zhang G, Zhong Y, Yang B, Hsu L-T (2024) A Framework for Graphical GNSS Multipath and NLOS Mitigation. *IEEE Transactions on Intelligent Transportation Systems* 25(9):12176 - 12186. <https://doi.org/10.1109/tits.2024.3374819>

## Author Biographies



**Sergio Vicenzo** is currently a Ph.D. candidate at the Department of Aeronautical and Aviation Engineering, The Hong Kong Polytechnic University. He received first-class honors in Bachelor of Engineering in Aviation Engineering from the same university in 2022. His research interests include GNSS urban navigation and positioning with direct position estimation.



**Bing Xu** received the BEng and Ph.D. degrees in network engineering and control science and engineering from the Nanjing University of Science and Technology, Nanjing, China, in 2012 and 2018, respectively. He is currently an Assistant Professor with the Department of Aeronautical and Aviation Engineering, The Hong Kong Polytechnic University. His current research interests include GNSS signal processing in software-defined global navigation satellite system receivers.